Response of a Tethered Zn-bis-Terpyridine Complex to an External Mechanical Force: A Computational Study of the Roles of the Tether and Solvent

Shouryo Ghose,[1] Anne-Sophie Duwez,[2] Charles-André Fustin,[3] and Françoise Remacle[1*]

1. Theoretical Physical Chemistry, Research Unit MOLSYS, University of Liège, 4000 Liège, Belgium
2. NANOCHEM, Research Unit MOLSYS, University of Liège, 4000 Liège, Belgium
3. Bio and Soft Matter division (BSMA), Institute of Condensed Matter and Nanosciences (IMCN), Université Catholique de Louvain, 1348 Louvain-la-Neuve, Belgium

Abstract

Polymeric material containing weak sacrificial bonds can be designed to engineer self-healing, higher toughness, improve melt-processing, or facilitate recycling. However, they usually exhibit lower mechanical strength and are subject to creep and fatigue. For improving their design, it is of interest to investigate their mechanical response at the molecular scale. We report on a computational study of the response to a mechanical external force of a Zinc (II) bis-methyl phenyl-terpyridine ($[Zn\text{-}bis\text{-}Terpy]^{2+}$) complex included in a cyclic poly(ethylene glycol) (PEG) tether designed to maintain the two partners of the metal-ligand bonds in close proximity after the rupture of the complex. The mechanical response is studied as a function of the pulling distortion using the CoGEF isometric protocol, including interactions with a polar solvent (DMSO). We show that tethering favors recombination but destabilizes the complex before bond rupture because of the interactions of the PEG units with the Terpy ligands. Similar effects occur between the DMSO molecules and the complex. Our results at the molecular scale are relevant for single-molecule force spectroscopy experiments. Interactions of the complex with solvent molecules and/or with the tether lead to a dispersion of the rupture force values which could obscure the interpretation of the results.

* Corresponding author email: fremacle@uliege.be

1. Introduction

Polymeric material containing weak sacrificial bonds can be designed to engineer much sought-after properties such as self-healing, response to stimuli, higher toughness, improved melt-processing, or facilitated recycling.[1-10] These properties arise from the ability of the weak bonds to break reversibly under an external mechanical force, thereby enabling the dissipation of the excess energy. The breaking of sacrificial bonds can be accompanied by the release of a hidden length which brings a reserve of extensibility upon stretching and can moreover help to maintain the two partners of the broken bond in close vicinity, favoring their recombination when the stress is relaxed. The concept of hidden length release upon breaking of weak bonds is abundantly exploited by nature to build materials with exceptional mechanical properties.[11-14]

Weak sacrificial bonds that rupture before the stronger ones of the polymeric materials in which they are embedded can be covalent bonds such as, e.g., Diels-Alder adducts, disulfide bonds, boronic esters, or imines,[6-9] or supramolecular bonds, e.g., H-bonds, pi-pi staking, or metal – ligand coordination bonds.[3, 4, 5] However, polymeric materials containing weak bonds present the drawbacks of their advantages: they have usually lower mechanical strength and are subject to creep and fatigue.[2, 15]

Studying their response at the atomic and molecular scale provides useful understanding towards the rational design of materials with better performances. Up to now, the mechanical response of weak bonds embedded in polymeric chains have been studied experimentally mostly by sonication experiments in solutions.[16-20] However, sonication experiments are limited in providing a detailed molecular response and quantitative information on the binding strength. Single-Molecule Force Spectroscopy (SMFS) is one of the methods that can provide quantitative information.[17, 21] It has been used to probe the strength of different types of bonds in various systems including covalent bonds,[22, 23] metal-ligands bonds,[24-26] bonds resulting from pericyclic reactions,[27-29] and interlocked architectures.[30-33] However, SMFS experiments remain very demanding, and it is therefore advantageous to model the response at the molecular scale using quantum chemistry approaches in order to guide future experiments.

Here, we investigate computationally the response to a mechanical external force of a Zinc(II) bis-methyl phenyl-terpyridine ([Zn-bis-Terpy]$^{2+}$) complex included in a cyclic poly(ethylene glycol) (PEG) tether that maintains the two partners of the metal-ligand bonds in close proximity after the rupture of the complex (Figure 1). The study is performed both in the gas phase and in a polar solvent (DMSO). Terpyridine is a ligand of choice because it can form complexes with a wide range of transition metal ions exhibiting varied thermodynamic and kinetic stability.[34] Terpyridine complexes have therefore been exploited in, e.g., catalysis,[35, 36] molecular motors,[37] sensing,[38, 39] and polymeric materials[40-44]. Zinc (II) was selected as metal ions because it forms rather weak and dynamic complexes with terpyridine and has been often used in metallo-supramolecular polymeric materials. Our aim is to characterize the mechanical properties of bis-terpyridine transition metal complexes, and to elucidate the influence of the PEG linker acting as a "tether" for the terpyridine ligands on these properties. Such tethered metal-ligand complex could indeed be used as sacrificial bonds allowing the release of hidden length in polymeric materials [14] and also for activation of latent catalysis [45, 46]. We compute the response to the external force at the molecular level at the *ab initio* quantum mechanical level using the CoGEF (COnstrained Geometries simulate External Force) isometric protocol.[47] We investigate the role of the tether and of the solvent on the ability of the complex to recombine after bond rupture free of mechanical constraint. Solvent effects are described by solvating the complex with solvent molecules at specific locations, as well as at the hybrid quantum

mechanics/classical mechanics QM/MM model [48] and with a polarizable continuous medium model (PCM).[49]

2. Computational Methods

2.1 Electronic structure

The electronic structure of the complex is computed at the spin restricted density functional theory (DFT) level of quantum chemistry method. using the Gaussian G16 computational package.[50] Range separated hybrid GGA[51] or meta-GGA/hybrid functionals,[52] as well as Grimme dispersion corrections,[53] are necessary to describe the range of interactions between the Zn^{2+} cation, the terpyridine ligands and the PEG tether that take place as the complex breaks under the external force. We selected the 6-31G(d,p) atomic basis set which offers a good comprise between accuracy and computer time. Overall, we get a good agreement between the results obtained with the ωB97xD[54] functional and M06-2X[52] functional. The ωB97xD/6-31G(d,p) level also leads to an equilibrium geometry of the [Zn-bis-Terpy]$^{2+}$ complex and to Zn-N and Zn-O bond strengths in agreement with previous works, see section 3 below. We therefore adopted the ωB97xD/6-31G(d,p) level for all the computations. More details about the selection of the functional and of the basis set are given in the supplementary information, SI, (Section S1, Table S1-S6 and Fig. S1). At the equilibrium geometries at zero force reported in the main text, all the frequencies are real.

2.2 Solvent effects

Typically, SMFS experiments are carried out in a solvent. Here, we investigate the effect of DMSO, a polar solvent in which the [Zn-bis-Terpy]$^{2+}$ complex is soluble. The solvent can play a crucial role in the response of the complex to the external force and in its reformation when the force is released, either by interacting directly with the complex or by forming a cage that could enhance or prevent the recombination step. DMSO can interact explicitly with the tethered complex by making H bonds with the C-H of the tether, by polarization interactions with the aromatic groups of the terpyridine ligands, or by interacting with the Zn^{2+} cation to form Zn-O bonds. Our computational results discussed below show that the strength of the Zn-O bond formed with DMSO is similar to that of the Zn-N bonds and also to the Zn-O bonds that can take place between the O atom of the PEG when the [Zn-bis-Terpy]$^{2+}$ complex is ruptured. Such bonds with Zn^{2+} have been previously reported for similar organic ligands.[55] For these reasons, we first investigated solvent effects by adding a few DMSO molecules to the complex in specific locations which provides qualitative trends since including a full layer of DMSO molecules to compute the mechanical response is computationally prohibitive. We also investigated solvation effects with the QM/MM-ONIOM (Our own N layered Integrated molecular Orbital and Molecular mechanics) electronic embedding methodology.[56, 57] For the QM part, we used two model systems, either the complex itself, or the complex with 6 interacting DMSO molecules. We find that overall, the QM/MM results are in agreement with the computationally less costly Polarizable Continuous Medium model (IEF-PCM)[58, 59] results when in the QM/MM approach the QM system comprises the complex only and no DMSO molecules. Because of its lower computational cost, we therefore used the PCM model to describe the effect of the DMSO on the complex in the majority of the reported results. More details about the solvation models used can be found in Section S2 of the SI, Fig. S2 to S4 and Tables S7 to S10. Throughout in the computations reported below, we neglect the effect of the counter ions, typically Cl^- which are expected to be well solvated and not interacting anymore with the complex in solution.

2.3 Response to an external mechanical force

Several theoretical methods have been developed to quantify the response of a molecular system to an external mechanical force.[60] The effect of the external force on the potential energy surface (PES) can be computed using quantum chemistry by an isometric or an isotensional approach. In the isometric method CoGEF (constrained geometries simulate external force)[47], a geometrical constraint is the control parameter. In the isotensional approach, the external force is explicitly added as a term in the expression of the nuclear gradient of the energy during the geometry optimization. Three isotensional approaches have been implemented, the force-modified-potential-energy surface (FMPES),[61] the external force is explicit included (EFEI)[62] and the enforce geometry optimization (EGO).[63] We adopt here the CoGEF approach. The constraint is the distance between the two pulling atoms to which the pulling force is applied (pulling distortion). The geometry is relaxed at each fixed value of pulling distortion leading to the FMPES. Since in this approach the external force is not applied directly, the force can be analyzed indirectly by monitoring the gradient on the nuclei at equilibrium under the constraint. Here, the pulling distortion is the distance between the two C atoms of the two terminal CH_3 groups, see Fig. 1a, and is parallel to the two axial Zn-N bonds, Zn-N_2 and Zn-N_5. The CoGEF calculations were carried out using Gaussian16 quantum chemistry packages.[50]

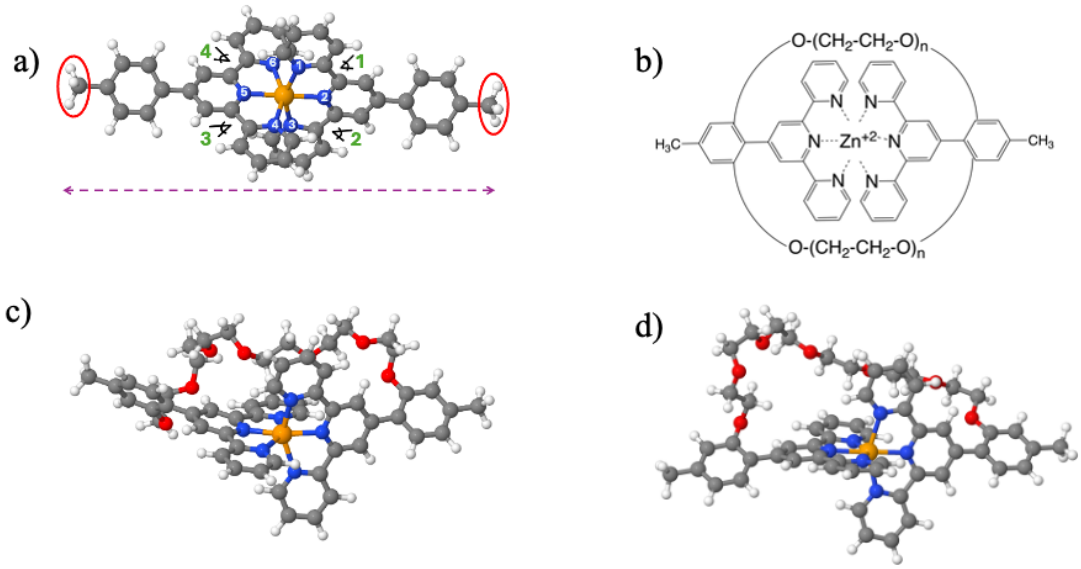

Fig 1: a) Equilibrium geometry in the gas phase of the untethered [Zn-bis-Terpy]$^{2+}$ complex. The ligand is 4'-(4-Methylphenyl)-2,2':6',2''- terpyridine. The pulling distortion is shown as a violet dashed line. It is applied to C atoms of the two CH_3 groups encircled in red. The coloring code of the atoms are: Zn in orange, N in blue, C in grey and H in white. Selected structural parameters are marked. The bonds Zn-N_1, Zn-N_3 , Zn-N_4, Zn-N_6 are equatorial bonds and Zn-N_2 and Zn-N_5 are axial bonds. Four dihedral angles between the pyridine units of the two ligands are numbered in green. The values of these parameters are reported in Tables 1 and 2 below. b) Schematic representation of the complex tethered with two oligomers of n PEG units. Equilibrium geometries in the gas phase of the two conformers of the one n=6 PEG tether complexes. c) Conformer A in which the PEG tether interacts with the Terpy ligands. d) Conformer B, for which the interactions are weaker, is higher in energy by 48 kJ/mol (free energy difference at 298 K).

3 Results and Discussion

4'-(4-Methylphenyl)-2,2':6',2''-terpyridine (referred as Terpy throughout, see Fig. 1) is a tridentate ligand. It binds to the metal ion through the N atoms of the 3 pyridine rings. At its free unbound equilibrium geometry, Terpy is in a trans planar conformation with two dihedral angles of ~ 0° between the pyridine units to avoid the repulsion between the lone pairs of N atoms. When Terpy binds with Zn^{2+} it undergoes a conformational transition from its trans planar structure to cis-planar structure. The destabilizing geometrical constraint on the two Terpy ligands is compensated by the formation of the 6 Zn-N bonds to obtain a stable [Zn-bis-Terpy]$^{2+}$ complex of approximate C_2 symmetry. In the complex, the two Terpy are perpendicular, so that the complex is achiral. At equilibrium geometry (ωB97xD/6-31G(d,p) level), the methyl phenyl group makes a dihedral angle of ~ 36° with the planar backbone of the terpyridine unit, which modifies the charge distribution on the N atom of the central pyridine. The octahedral coordination sphere of the Zn cation is slightly distorted with the two axial bonds shorter than the 4 equatorial bonds, see Table 1 and Fig. 1a. The computed equilibrium geometries of the [Zn-bis-Terpy]$^{2+}$in the gas phase and in DMSO are in good agreement with computed and crystallographic structure data.[64-66] Note however that angles and bond lengths differ because of the packing environment in the crystal. The strength of the three Zn-N bonds formed by ligation with a Terpy ligand can be estimated from the thermochemistry of the reaction $[\mathrm{Zn-bis-Terpy}]^{2+} \rightarrow [\mathrm{Zn-Terpy}]^{2+} + \mathrm{Terpy}$. We obtain a ΔE at 0K = 573.51 kJ/mol. The free energy difference is ΔG^0 at 298 K is 516.51 kJ/mol. This gives an approximation of the Zn-N bond strength of ≈ 200 kJ/mol.

3.1 Impact of the tether on the equilibrium geometry of the complex at zero force

The PEG tether is attached on the phenyl group of the Terpy ligands in ortho position. Since all the dihedral angles and bond angles of the PEG tether are free, there are multiple quasi energetic local minima that can be populated at room temperature. One expects the conformation of the PEG chain and strength of its interaction with the Zn complex will affect the CoGEF potential profiles and the rupture force. Similar results in families of stable conformers are expected for the one n=6 and one n=8 tether complexes. The geometry of the two n=6 tether complex is more rigid. For these reasons, in view of convergence issues encountered computing the CoGEF profiles and limitations in computer time resources, a systematic conformer search was carried out only for the one n=6 tether complex. We use the CREST (Conformer-Rotamer Ensemble Sampling Tool) [67, 68] at the semi empirical gfn2-xTB level of electronic structure[69, 70] see SI, section S3 and Fig. S5 for more details. The equilibrium geometries of the lowest conformer was then recomputed at the ωB97xD/6-31G(d,p) level, as well as the CoGEF potential curves. We find that there are two families of conformers. In the lowest one, Fig. 1c, conformer A, the PEG chain is somewhat twisted and interacts with an equatorial pyridine of each Terpy ligand. Throughout the paper, by 'equatorial' pyridine, we mean a pyridine that contains a N atom involved in an equatorial Zn-N bond, N_1, N_3, N_4, N_6. Conversely, by axial pyridine, we mean a pyridine that contains the N atom of an axial Zn-N bond, N_2 or N_5. Conformers where the PEG chain only weakly interacts with the [Zn-bis-Terpy]$^{2+}$ complex are significantly higher in energy. The conformer of this type retained in this study is 68.42 kJ/mol higher in energy than the lowest identified conformer (Conformer B, Fig. 1d). As discussed below, the stronger the interaction, the more distorted the coordination shell of the Zn complex, which leads to different mechanical response. We therefore report on both conformers below. For the one n=8 tether complex, we retained a conformer (Fig. 2a) where the PEG unit interacts with an equatorial pyridine of one Terpy ligand. The values of the geometrical parameters marked in Fig. 1a are reported in Table 1 for free and selected tethered complexes in gas phase.

Table 1: Selected bond length (Å) and angle values (degrees) of the complex without tether and tethered with n=6 or n=8 PEG chains in the gas phase. Zn-N_2 and Zn-N_5 are the axial bonds.

	Free complex	One n=6 tether (conf. A)	One n=6 tether (conf. B)	Two n=6 tethers	One n=8 tether
Zn-N_1	2.17	2.24	2.17	2.17	2.15
Zn-N_2	2.08	2.06	2.07	2.09	2.07
Zn-N_3	2.17	2.18	2.18	2.21	2.23
Zn-N_4	2.17	2.17	2.17	2.15	2.16
Zn-N_5	2.08	2.08	2.07	2.07	2.07
Zn-N_6	2.17	2.18	2.18	2.19	2.20
Angle 1	0.13	-12.40	-9.71	6.99	-5.91
Angle 2	0.11	6.46	8.30	-5.53	5.52
Angle 3	0.16	14.53	-5.94	-1.86	-9.46
Angle 4	0.08	-15.51	10.08	-6.15	8.64
<N_2-Zn-N_5	179.97	165.37	176.69	173.40	171.94

The incorporation of the tether increases the distortion of the octahedral symmetry of the complex. These structural changes vary depending on the orientation of the tether with respect to the Zn-N sphere moiety. As shown above, the free complex has four equatorial Zn-N bonds and two shorter axial bonds of equal length. For the one n=6 conformer A , which is the lowest energy conformers, the PEG chain is twisted and interacts through its O atoms with the Π electron cloud of an equatorial pyridine of each Terpy ligand, which distorts the coordination of the Zn complex and lead to a significant relaxation of the cis planar geometry of the Terpy ligand to a twisted form and small changes in the Zn-N bond lengths at zero force equilibrium geometry (Fig. 1c). As a result, the dihedral angles 1 to 4 significantly increase as well as the equatorial Zn-N_1 bond length, see Table 1. In the one n=6 conformer B which is higher in energy by 68.42 kJ/mol ($\Delta G = 48.47$ kJ/mol), the PEG chain does not interact with the complex and the Zn-N bond lengths remain essentially unchanged compared to the free complex. For the longer, one n=8 tether, we retained a conformer for which there is an interaction between the O atom of the PEG chain with the Π electron cloud of only one equatorial pyridine of the

Terpy ligand, see Fig. 2a. This interaction leads to similar but weaker distortion of the Zn complex compared to the one n=6 Conformer A. In Section S3, Figure S5, Tables S12 and S13, we report structural properties of other one n=6 and one n=8 tethered conformers.

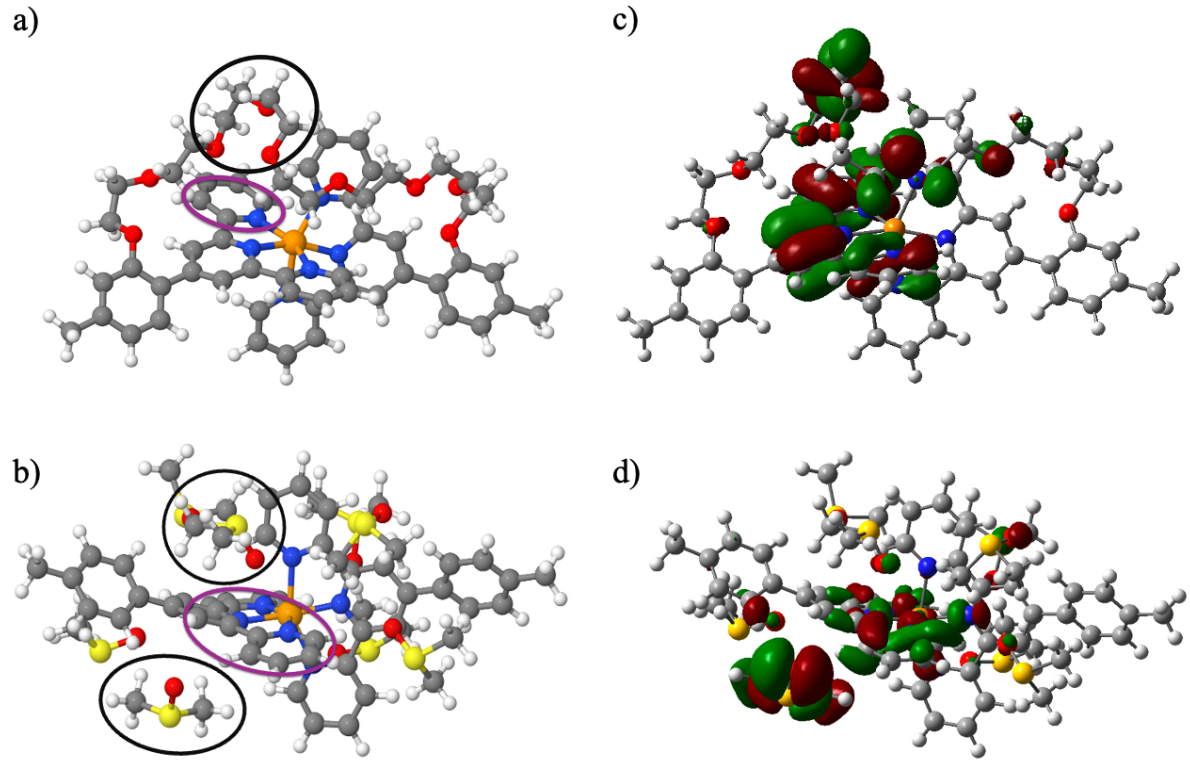

Fig 2: a) Example of interaction between a folded portion of the n=8 PEG tether (black circle) and the equatorial pyridine of the Terpy ligand (violet circle). b) Example of interaction of the free complex with DMSO molecules (encircled in black) and the pyridine units encircled in violet (equilibrium geometry of a $[Zn\text{-bis-Terpy}]^{2+}$ - 8 DMSO complex), see Fig. S3 for the interaction between DMSO and the PEG chain by weak H-bonding. c) Isocontour of the HOMO-8 of the n=8 tether complex shown in panel a, lying 1.28 eV below the HOMO, which is localized on the $[Zn\text{-bis-Terpy}]^{2+}$ complex and on the PEG tether. d) Isocontour of HOMO-8 of the $[Zn\text{-bis-Terpy}]^{2+}$ - 8 DMSO complex shown in panel b), lying 0.56 eV below the HOMO, which is localized on DMSO molecules and on the complex. The isocontour value is 0.02.

The structural changes discussed above reflect the changes in the electronic structure induced by tethering the complex, i.e., both the substitution on the phenyl ring by the terminal O atom of the tether and the polarization interactions between the tether and the terpyridine ligands. In the free complex at zero force whose equilibrium geometry is shown in Fig. 1a, the HOMO (184) and HOMO-1 (183) are degenerate, have a bonding Π character and mainly localize on the 'axial' pyridine of the Terpy ligands and on the adjacent phenyl groups, see Fig. 3c. These two orbitals are also localized to a lesser extent over the entire molecular backbone, including the axial Zn-N bonds. The LUMO and LUMO+1 are degenerate and localized on the Terpy ligands and on the adjacent phenyl group. The frontier MOs are non-bonding with Zn^{2+}. The most stable Zn-N bonding orbital is MO 155 (HOMO-29), at 4.51 eV below the HOMO. It is bonding for the 6 Zn-N bonds and is fully symmetric. Upper in energy, there is MO 158 (3.77 eV below the HOMO), which is bonding for the two axial bonds with a change of phase, and MO 164 (3.41 eV below HOMO) and MO 163 (3.42 eV below HOMO) which are bonding

along the equatorial bonds with different phases. See Figure S8 of the SI. In contrast, because the tethering breaks symmetry, the HOMO and HOMO-1 are no longer degenerate, see Fig. 3c and e), and no longer delocalized over the entire molecular backbone in the one n=6 tethered complex of conformer B. They are localized on the methyl-phenyl anchoring groups on each side with some delocalization on the adjacent PEG units. The LUMO and LUMO+1 (Fig. 3d and f)) remain localized on the [Zn-bis-Terpy]$^{2+}$ complex but their degeneracy is lifted, and their symmetry broken. The bonding Zn-N MO's have some localization on neighboring PEG units of the tether which reflects the polarization interactions between the O of the tether and the Terpy ligands, see Figure S9. The polarization interaction between the PEG chain and the complex are also reflected in the delocalization of bonding MO's over the complex and neighboring PEG units, as shown in Fig. 2c for the HOMO-8 of the one n=8 tether complex.

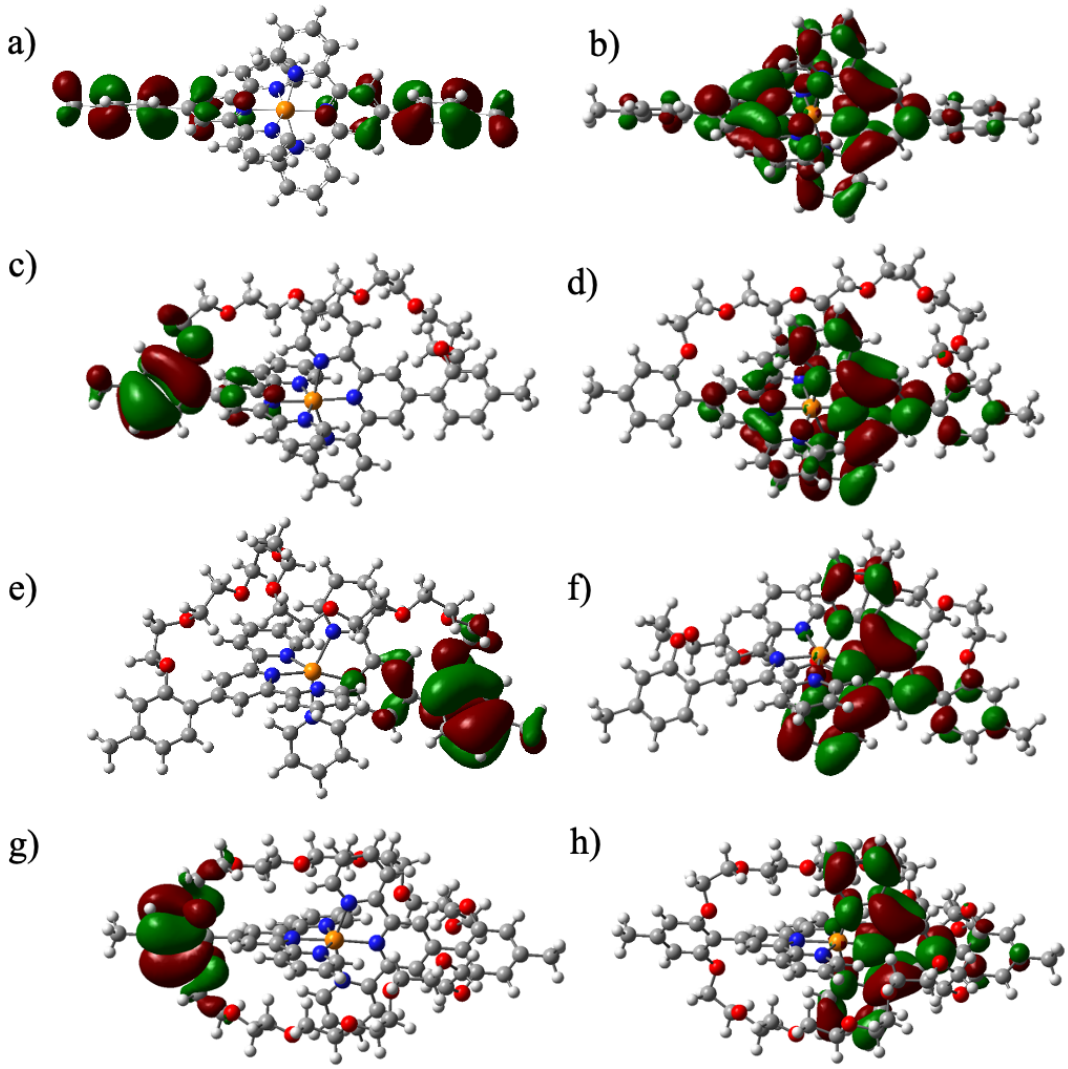

Figure 3. HOMO and LUMO isocontours of the free complex (a) and (b). Note that for the free complex HOMO-1 (not shown) is degenerate with the HOMO, and LUMO+1(not shown) with the LUMO. This degeneracy is lifted when the complex is tethered. c) and d) are the isocontours of the HOMO and the LUMO of the one n=6 conformer B complex and e) and f) of its HOMO-1 and LUMO +1. g) and h) are the isocontours of the HOMO and the LUMO of the two n=6 tether complex. The isocontour value is 0.02.

3.2 Solvent effects at zero force

We investigate solvent effects with a relatively polar solvent, DMSO (ε = 46.83). Partially explicit solvation effects are studied by relaxing the geometry of the free complex interacting with 8 DMSO molecules. Very much in the same way as the PEG units of the tether, individual DMSO molecules can polarize the Terpy ligands, see Fig. 2b and d, for the equilibrium geometry of the [Zn-bis-Terpy]$^{2+}$ with 8 DMSO molecules. In addition, our results show that DMSO can also complex the Zn^{2+} cation but thermodynamically, cannot displace the Terpy ligands at zero force. The computed standard free energy difference, $\Delta G^0$of the reaction $[\mathrm{Zn(DMSO)_6}]^{2+} + 2\ \mathrm{Terpy} \rightarrow [\mathrm{Zn-bis-Terpy}]^{2+} + 6\ \mathrm{DMSO}$ is -136.68 kJ/mol in the gas phase, see SI (section S2.4) for additional details. In addition, DMSO molecules can interact with the PEG units of the tether through weak H bonds between the O of DMSO with the H atoms in the PEG chain, and through polarization interactions with the terpyridine ligand see Fig. S3. Solvent effects were also studied with the PCM model and at the QM/MM level with ONIOM. Details on the construction of the solvent layers around the complex for the ONIOM solvation model are given in the SI (Section S2, Fig. S2), we only report in the main text results for which the QM model does not include explicitly DMSO molecules. The equilibrium geometries of the free complex and of the tethered complexes computed at the PCM and at the ONIOM levels are very similar to those of the gas phase plotted in Fig. 1a, d and in Fig. 2a. We report the values of the selected structural parameters in Table 2 for the PCM model.

Table 2: Selected bond lengths, bond angles and dihedral angles of the complex (see Fig. 1a) without tether and with one or two n=6 tether in different solvation models.

	Free complex PCM	Complex + 8 DMSO	One n=6 PCM (conf. B)	Two n=6 PCM
Zn-N_1	2.16	2.16	2.17	2.17
Zn-N_2	2.08	2.06	2.08	2.09
Zn-N_3	2.16	2.15	2.17	2.21
Zn-N_4	2.16	2.26	2.16	2.15
Zn-N_5	2.08	2.07	2.08	2.07
Zn-N_6	2.16	2.17	2.19	2.19
Angle 1	-1.54	2.87	-8.31	6.99
Angle 2	-0.91	-5.29	8.49	-5.53
Angle 3	-1.57	22.38	-6.37	-1.86

Angle 4	-0.88	-20.64	11.90	-6.15
$<N_2$-Zn-N_5	179.91	162.24	176.22	173.40

As can be seen by comparing Tables 1 and 2, PCM solvation does not significantly affect the structural parameters of the complex, while explicit solvation by 8 DMSO molecules (see Fig. 2b) affects the values of the dihedral angles, and the Zn-N bond lengths involved in the Terpy ligand that interacts with a DMSO molecule. There is also no significant structural change in the tethered complex at the PCM level. The same is true for the results of the ONIOM model reported in the Table S8 of the SI.

3.3 Mechanical response in the gas phase and solution

We now discuss the effect of the tether on the mechanical response of the complex, summarized in Figure 4. We report the response of the free complex (Fig. 1a) and one n=6 conformer A (Fig. 1c), of the one n=8 tether complex (Fig. 2a) and two n=6 tether complex (Fig. 3g). The CoGEF potential energy curves as a function of the pulling distortion in the gas phase and solution are plotted in Figs. 4a and 4f. The geometries of the complexes at the last point before bond rupture are shown in Figs. 4 b-e and g-j. The geometries of the complexes at the first point after bond rupture are reported in Fig. S11. The corresponding force on the pulling atoms are given in Fig. S14 and Table 3 below.

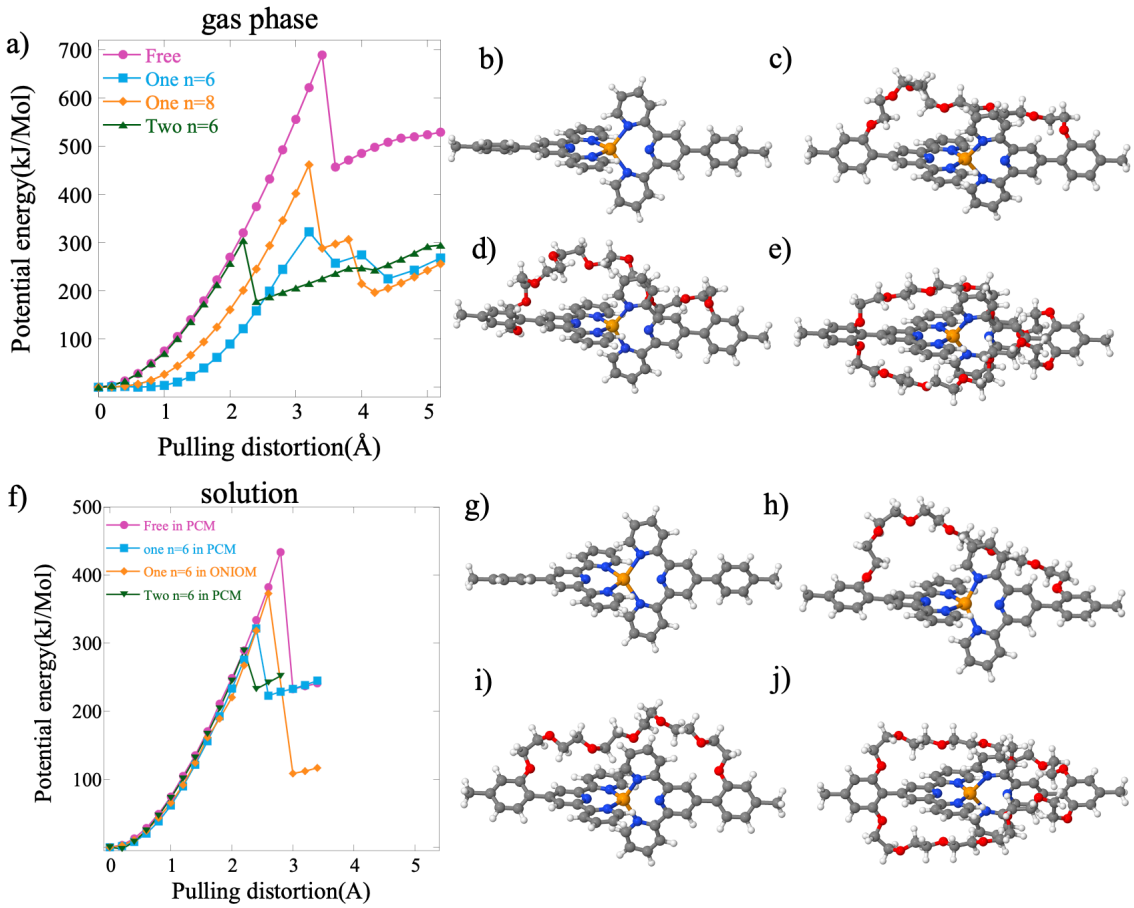

Figure 4. Computed mechanical response of the free complex, of the one n=6 (Conformer A), of the one n=8 tether, and of the two n=6 tether complexes in the gas phase (panels a to e) and in solution (panels f to j). Panel a) CoGEF potential energy curves, b to e: Equilibrium geometries at a pulling distance just before bond rupture for the free complex (b), complex with one n=6 conformer A (c), complex with one n=8 tether (d) and complex with two n=6 tethers (e). f) CoGEF potential energy curves for PCM solvation model g) Equilibrium geometries just before bond rupture of the free complex at the PCM level. The complex with one n=6 in (h) PCM and (i) ONIOM. j) the complex with two n=6 tethers in PCM.

Table 3: Values of the pulling distortion(Å) before the rupture and the force on the pulling atoms for the free and tethered complexes in gas and solvent phase.

	Pulling distortion (Å)	F_{max} (nN)
Free in gas phase	3.4	5.81
One n=6 (conf. A) in gas phase	3.2	4.35
One n=8 in gas phase	3.2	5.07
Two n=6 in gas phase	2.2	4.11
Free in PCM	2.8	4.36
One n=6 in PCM	2.4	3.95
One n=6 in ONIOM	2.6	4.39
Two n=6 in PCM	2.2	3.85

As can be seen from Fig. 4a and reported in Table 3, in the gas phase, the free complex breaks at a pulling distortion of 3.4 Å which corresponds to a force of 5.81 nN on the pulling atoms. Just before rupture, the value of the potential energy is ≈ 700 kJ/mol. The tethered complexes break at lower force values (4.0 - 5.2 nN) and shorter pulling distortions (between 2.2 and 3.2 Å) because of the destabilization due to the polarization and H-bond interactions between the Terpy ligands and the PEG units as discussed in Section 3.1 above (see also Figs. 1c, 2a and 2c). The CoGEF potential profile of the one n=6 conformer A (Fig. 1c) where there is a stronger interaction with the Terpy ligands breaks for a lower value of the potential energy (≈ 300 kJ/mol) than the one n=8 tether (≈ 450 kJ/mol) and at a lower force of 4.35 nN, see Table 3. The one n=6 tether conformer B (see Figure S6) behaves in a similar way as the one n=8 tether complex. The complex with two n=6 tethers is significantly more destabilized than the complexes with one n=6 tether conformer B and one n=8 tether. Curves corresponding to slightly different conformations are reported in the SI (Fig. S6). While not identical, they obey the same trends. The values of the rupture forces reported in Table 3 are in the range of 3.85

for the two n=6 tether complex in solution to 5.85 nN for the free complex. They are in the range of those computed for the rupture of other types of weak covalent bonds but often higher than the measured ones because typically the role of the polymer linker in which the mechanophore is embedded is not taken into account in the simulations, see for example[24, 26, 28, 61, 62, 71-75].

Upon rupture of the free complex, only three Zn-N bonds are broken, see Fig. S11, which explains that only ≈ 200 kJ/mol are released. For the free complex, the value of the pulling distortion just before bond breaking is 3.4 Å which corresponds to an energy difference with the zero force equilibrium energy of ≈ 700 kJ/mol. The energy of the next point which corresponds to weakly interacting $[Zn\text{-}Terpy]^{2+}$ and Terpy fragments ~ 456 kJ/mol. As the pulling distortion continues to increase, one is reaching 528 kJ/mol at 5.2 Å which almost corresponds to the energy difference of 573 kJ/mol of the reaction $[Zn\text{-}Terpy]^{2+}$ + Terpy reported in section 2.1. The Zn^{2+} cation forms a planar $[Zn\text{-}Terpy]^{2+}$ mono-complex and the other Terpy ligand undergoes a geometry change from cis-planar to a cis-non-planar geometry. Reaching the equilibrium trans conformation requires a larger separation between the two moieties. The two Terpy ligands maintain an almost perpendicular orientation with respect to one another. The pulling distortion modifies the localization of the MOs along the molecular backbone. As it increases, the HOMO and HOMO-1, shown in Fig. 3a at zero force, are no longer degenerate and localize more and more each on one side of the complex. At step 16 (pulling distortion = 3Å), they are destabilized by 0.22 eV. Upon stretching, the Zn-N bonds are also reorganized. At step 18, just before bond breaking, MO 156 (bonding for both axial and equatorial bonds) is destabilized by 0.22 eV and the two Zn-N axial bonds are considerably weakened (elongated by 0.93 Å), see Fig. S10. On the other hand, the equatorial bonds are much less destabilized and elongated only by 0.12 Å. In Fig S12 we show the variation of the energies of the set of MO's HOMO-12 to HOMO-19 for free complex with increasing pulling distortions. Among this set, the σ type MO of the methyl phenyl groups are destabilized (≈ 0.3 eV) which is accompanied by an elongation of the C-C bonds parallel to the pulling distortion.

The tethered complexes also break into a Terpy moiety that goes back to its twisted cis form and a $[Zn\text{-}Terpy]^{+2}$ mono-complex, which both remain attached to the PEG tether as targeted by the design. The Terpy moiety remains roughly perpendicular to the plane of the $[Zn\text{-}Terpy]^{2+}$ mono-complex as for the untethered complex. The difference with the untethered complex is that O atoms of the PEG chain can interact with the Zn^{2+} cation, which stabilizes the $[Zn\text{-}Terpy]^{+2}$ mono-complex. In the case of the one n=6 conformer B, the configuration of the PEG chain is such that two Zn-O bonds are formed leading to a 5 coordination of the Zn^{2+}, see Fig S11b. Three and five coordination complexes of the Zn^{2+} cation have been previously reported.[76] In the case of the n=8 complex, for the PEG conformation shown here, only one Zn-O bond is formed, leading to a distorted tetrahedral geometry. Overall, the free complex is more stable under a pulling force than the tethered ones before rupture, but after rupture the $[Zn\text{-}Terpy]^{+2}$ mono-complex is stabilized by the formation of the extra Zn-O bonds with the PEG chain.

The effect of the solvent on the mechanical response is to further destabilize the complex, as shown by the CoGEF curves for the free complex in PCM. The mechanical responses of complex with one n=6 tether, computed in PCM and in ONIOM, and of the complex with two n=6 tethers are plotted in Fig. 4f, see also Table 3. The PCM solvated untethered complex breaks at a lower value of pulling distortion (2.8 Å) that corresponds a lower value of the potential energy under force (450 kJ/mol). The release of energy after bond rupture due to the moieties relaxation is ≈ 200 kJ/mol, similar to that observed in the gas phase. The tethered complexes remain destabilized with respect to the untethered ones in solution as in the gas

phase and break at lower values of the pulling distortion. In all complexes in solution, the Terpy ligand of the [Zn-Terpy]$^{2+}$ mono-complex remains almost perpendicular to the released Terpy ligand. In the ONIOM model for solvation, the solvent molecules have more flexibility to reorient as the pulling distortion increases, and as a result, the complex is more effectively solvated in the ONIOM model than accounted for by distortion of the cavity in the PCM model. This results in a smaller destabilization of the complex with one n=6 tether at the ONIOM level compared to PCM model results.

Compared to the gas phase, there is a significant difference in the equilibrium geometries under force after bond rupture for the tethered complexes where the two moieties are still weakly interacting (Fig S11 panel e-h). The electrostatic interactions of the PEG oligomer with the solvent, included as a polarization medium in the PCM model, prevent the interaction between the O of the PEG units and the Zn cation after bond rupture. The same is true in the ONIOM model. As can be seen for Fig. S11 f, g and h, in all cases, a 3 coordination [Zn-Terpy]$^{2+}$ mono-complex is formed, without additional interactions with the PEG units. The other Terpy ligand relaxes and adopts a cis twisted geometry, roughly perpendicular to the Terpy of [Zn-Terpy]$^{2+}$ mono-complex. Note that in the ONIOM model, the conformation of the PEG chain after bond rupture changes with respect to the gas phase (Fig. S11g after rupture) while it remains similar in PCM.

4. Release of hidden length after bond rupture

After bond rupture, the external mechanical force unfolds the tethering PEG oligomer, releasing its hidden length. In SMFS experiments,[28] the hidden length is defined as the distance between the surface and the cantilever. Since in the CoGEF protocol, the distance between the pulling atoms is applied as a geometrical constraint, we report in Figure 5 below the distance O-O between the anchoring units of the PEG chain on the terminal phenyl group of the complex as well as the length of the 6 Zn-N bonds of the complex. In Figure 5a, we show the 6 Zn-N bond lengths as a function of the pulling distortion of the free complex for reference. Since the force direction projcts better on the axial bonds (Zn-N_2 and Zn-N_5), they are the most elongated, reaching 3.16 Å just before rupture (3.4 Å of pulling distortion). On the other hand, the pulling force is essentially perpendicular to the equatorial bonds whose lengths do not vary significantly. They reach 2.36 Å at 3.4Å of pulling distortion. After the bond rupture, there is a reorganization of the Zn-N bonds, with three essentially identical Zn-N bonds in the [Zn-Terpy]$^{+2}$ complex (Zn-N_4,, Zn-N_5 and Zn-N_6 at 1.96 Å) and three long ones (Zn-N_1,, Zn-N_2 and Zn-N_2) for the three N atoms of the Terpy ligand, which continue to increase with the pulling distortion.

In the tethered complexes, upon stretching, the O-O distance increases linearly with the pulling distance for the one n=6 conformers A and B, see Fig. 5 b and d. The increase of O-O distance in conformer A occurs in two steps. The direction of the force is not parallel to the axial bonds at zero force. The stretching first induces a reorganization of the conformation of the PEG chain (at 0.5 Å) with a breaking of the interactions with the Terpy ligands and an alignment of the Zn-N axial bonds with the force. Then the three Zn-N bond that will break begin to extend and the O-O distance increases monotonically, except for a small kink due to Zn-O interactions with the [Zn-Terpy]$^{2+}$ after the rupture of the three Zn-N bonds. At large pulling distortion, the PEG chain is stretched, the O-O distance reaches a length of 18Å, with an increase of ≈ 14.5 Å compared to the zero force value. In conformer B, the axial Zn-N bonds are parallel to the pulling distortion and the extension of the PEG chain under force has a different profile. There is a 2.5 Å release of length in the O-O distance at the rupture of the three Zn-N bonds (at 3Å)

followed by a linear increase, to reach 18.5 Å at 7Å of pulling distortion. The geometry of the extended PEG stretched conformer B is shown Fig. 5f. Note that at the bond rupture, Zn-N bonds of conformer A extend less (to ≈ 4.5Å) than those of conformer B (≈ 5.8 Å). Both extensions are smaller than in the free complex (≈ 7Å, Fig. 5a). The increase of the O-O distance in the one n=8 tether complex is monotonic, with a small step (0.5 A) at 3.2 Å before the bond rupture, see Fig. S13, which also shows the response of the bond lengths of the one n=6 tether complexes in solution. The bond response of the two n=6 tether is plotted in Fig. 5c and its extended geometry in Fig. 5e. The extension of the O-O distance is similar to those of the other tether complexes and that of the Z-N bond at rupture to those of the one n=6 tether. The values of the force on the pulling atoms as a function of the pulling distortion reflect the mechanical response of the bond lengths, see Fig. S14.

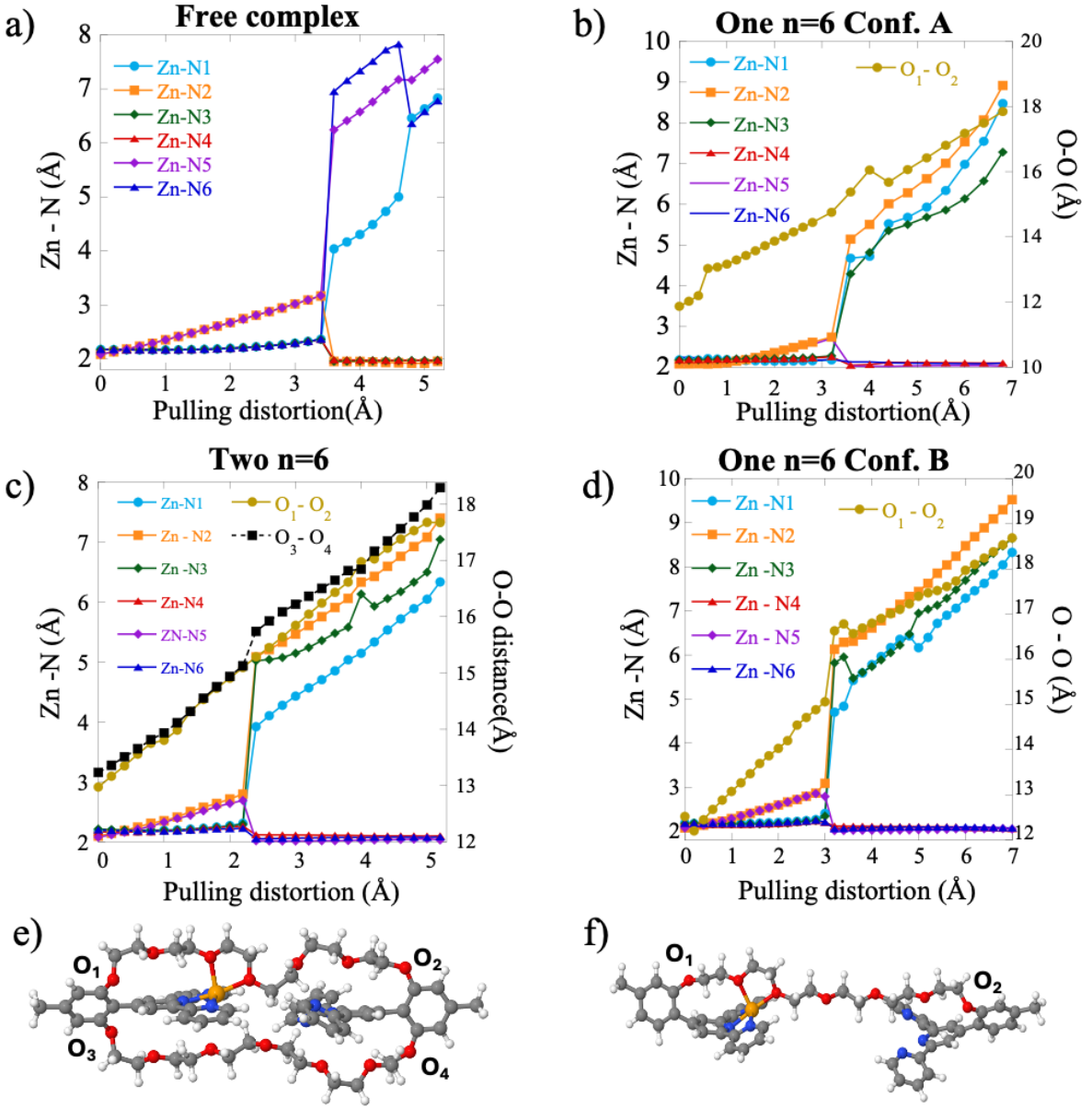

Figure 5. Release of hidden length. a) to d) The O-O distance between the anchoring PEG units and the six Zn-N bonds as a function of the pulling distortion for the free complex (a), for the one n=6 tether conformer A (b), two n=6 tether (c) and one n=6 tether conformer B (d)

computed in the gas phase. Equilibrium geometries of two n=6 tether complex in gas phase at 5Å of pulling distortion (e), and of one n=6 tether conformer B at 10 Å, see Fig. S13 for the one n=8 tether complex in the gas phase and n=6 one and two tether in solution. The force on the pulling atoms as a function of the pulling distortion for the one n=6, one n=8 and two n=6 complexes in gas phase and one n=6 tethered complex in PCM are shown Fig. S14.

5. Effect of the tether and solvent on the recombination of the complex

We investigated how the presence of the solvent and/or of the tether influences the recombination once the pulling distortion is released after bond breaking. For doing so, we removed the geometrical constraint on the equilibrium geometries obtained under force after bond rupture shown in Fig. 4. The results are summarized in Fig. 6. Overall, all the complexes recombine to the same equilibrium geometry as the one determined at zero force (gas phase and PCM, Fig. 6a), or to a different local minimum conformer with either a higher or lower energy (tethered complexes in the gas phase and in solution, Fig. 6b to f). For one n=6 tethered complex of Conformer A in gas phase the relaxation of the pulling distortion leads to a six coordinated [Zn-bis-Terpy]$^{+2}$ is very close to its equilibrium force free geometry (ΔG= -0.59 kJ/mol, Fig. 6b). For conformer B, the relaxation of the pulling distortion leads to a less stable (ΔG = -109.38 kJ/mol) 5 coordinated [Zn-Terpy]$^{2+}$ complex where a PEG unit makes two Zn-O bonds and the other Terpy ligand remains unbound, see Fig S15a. For the complex with one n=8 in the gas phase (Fig. 6c), the relaxation of the pulling distortion leads to a less stable (ΔG -87.09 kJ/mol) 6 coordinated [Zn-Terpy]$^{2+}$ complex where a PEG unit make one Zn-O bond and only one pyridine of the other Terpy ligand remains unbound. Since the ΔG for the isomerization from these geometries to the initial 6 coordinated [Zn-bis-Terpy]$^{2+}$ is negative, the complex will eventually revert to its initial geometry. This isomerization implies a change in the conformation of the PEG tether and of the unbound Terpy ligand that needs to be planar for forming the 6 coordinated complex. It was not possible to estimate a transition state and therefore we do not have access to the kinetics of this isomerization. For the complex with two n=6 tethers in the gas phase (Fig. 6d), upon relaxation of the force, the geometry converges to a 6 coordinated [Zn-bis-Terpy]$^{2+}$ complex slightly more stable than the initial one (ΔG=6.74 kJ/mol, Fig. 6d). Selected parameters are reported in SI, Section S3 (Fig S7, Table S14) as well as the CoGEF curve, which is very similar to that of Fig. 4a. The relaxed complexes with one n=6 tether in solution (PCM model) after bond rupture, Fig. 6e is also found to be slightly more stable that the initial conformer (ΔG= 16.10 kJ/mol), while the two n=6 tether is slightly less stable (ΔG=-5.14 kJ/mol). These results suggest that the geometrical constraints due either to the presence of two tethers in the gas phase or of the solvent cage facilitate the recombination to a 6 coordinated [Zn-bis-Terpy]$^{2+}$ complex with 6 Zn-N bonds. The recombination to the initial 6 coordinated [Zn-bis-Terpy]$^{2+}$ complex also occurs for the ONIOM solvation model as well as for explicit solvation models, see SI, Fig. S15b to d.

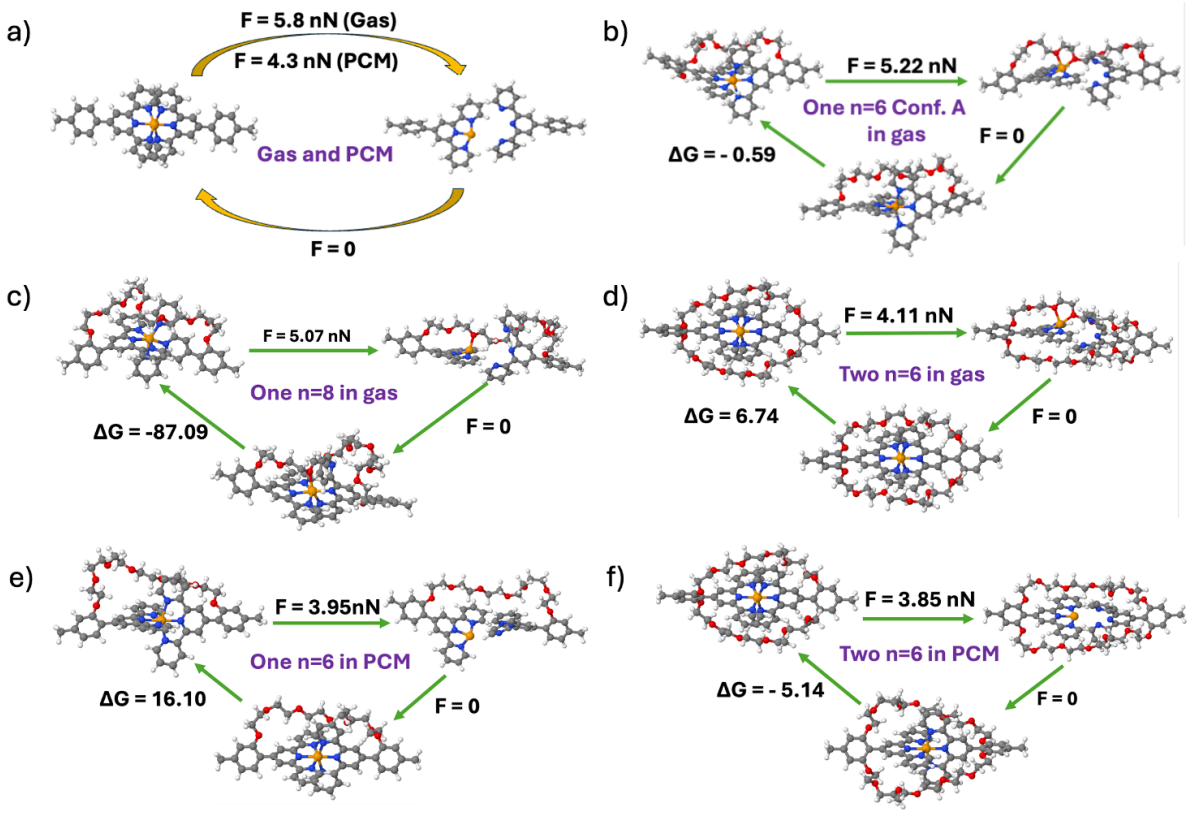

Figure 6. Rupture-Recombination cycle for selected complexes as indicated.

6. Concluding remarks and perspectives

Our computational study aimed to shed light on the mechanical response of a metal-ligand complex-based mechanophore, the 6-coordinated [Zn-bis-Terpy]$^{2+}$ complex, and to investigate the role of tethering the complex with one or two PEG oligomers on the rupture and recombination processes in the gas phase and in a polar solvent in which the complex is soluble (DMSO). Both the O atoms of the PEG tether and of DMSO can form Zn-O bond that are however less stable than the Zn-N ones. Solvent effects were investigated at the PCM and ONIOM model and using explicit solvation with a few DMSO molecules.

In the [Zn-bisTerpy]$^{2+}$ complex at equilibrium geometry, the two Terpy ligands adopt a cis planar conformation so that the complex can be stabilized by 6 Zn-N bonds with the two planes of the Terpy ligands oriented perpendicularly to one another. Tethering the complex with one or two PEG oligomers slightly destabilizes the 6-coordination sphere of [Zn-bis-Terpy]$^{2+}$ because of the polarization interactions between the PEG units and the pyridine cycles. Depending on the conformation of the PEG oligomers, the strength of the interactions differs, which leads to the coexistence of several isomers of the tethered complexes close in energy.

We studied the effect of an external force using the isometric CoGEF approach which provides the potential energy curves as a function of the applied pulling distortion that stretches the complex along its two axial bonds. We found that upon rupture of the free complex, a planar 3 coordinated [Zn-Terpy]$^{2+}$ mono-complex is formed and that the freed Terpy ligand isomerizes to a more stable twisted cis geometry, both in the gas phase and in the PCM or ONIOM models of solvation. After bond rupture, in the tethered complexes, both in the gas phase and solvated,

the O atoms of the PEG units can stabilize the [Zn-Terpy]$^{2+}$ mono-complex by forming Zn-O bonds, which leads to 4 or 5 coordinated Zn complexes. Zn-O bonds can also be formed with the [Zn-Terpy]$^{2+}$ mono-complex for complexes solvated explicitly by DMSO molecules. Explicit solvation with DMSO molecules, conformation of the PEG chain, and the resulting interaction between the PEG chain and the Terpy ligands lead to a dispersion of the values of the pulling distortion, and therefore of the force, at which the complex ruptures. While conformers exhibiting a strong interaction between the PEG chain and the [Zn^{2+}-bis-Terpy] complex are overall stabilized, the interaction destabilizes the Zn coordination sphere which leads to lower rupture forces provided that the interaction does not modify significantly the orientation of the axial Zn-N bond with respect to the pulling distortion.

After bond rupture, gas phase and PCM solvated free complexes recombine to a 6 coordinated [Zn-bis-Terpy]$^{2+}$ when the pulling distortion is relaxed. The tethered solvated complexes, in the gas phase and in PCM and ONIOM solvation models, also recombine. They can however form a complex with a different conformation of the PEG chain which can be more stable or less stable than the initial geometry. Complexes with one tether in the gas phase or solvated explicitly with DMSO molecules do not necessarily recombine to a 6 coordinated [Zn-bis-Terpy]$^{2+}$. Rather, the unstable 4 or 5 coordinated [Zn-Terpy]$^{2+}$ complex relaxes to a metastable conformer where the second Terpy ligand remains in a cis non-planar form and is only making 1 or 2 Zn-N bonds. This conformer is however higher in energy than the coordinated [Zn-bis-Terpy]$^{2+}$ which is the thermodynamically stable species.

Our study suggests that solvation may suffice to ensure that the two parts of the complex after bond rupture remain in close enough vicinity to recombine when the pulling distortion is relaxed. However, if the solvent molecules interact too strongly with the metal cation, 'hybrid' metastable complexes can form, whose lifetimes may be long. Tethering the complex with two PEG linkers also provides a cage that favors the recombination of the two parts when the pulling distortion is relaxed after bond rupture. Both the interactions with the PEG oligomer and with a solvent destabilize the complex. When only one tether is used in the gas phase, the O atoms of the PEG oligomer can form Zn-O very much in the same way as with DMSO molecules, which leads after bond rupture to metastable 'hybrid' complexes. When the tethered complex is solvated, the interactions between the PEG oligomer and the solvent prevent this kind of complex from forming.

Our results confirm that tethering favors recombination and shed light on the role of the tether at the atomic scale. They provide useful physical insights to the mechanical response of polymeric materials with tethered sacrificial bonds and pave the way for SMFS experiments. Too strong interactions of the complex with solvent molecules and/or with the tether modify the rupture and recombination processes and lead to a dispersion of the rupture force values and hidden length release which could obscure the interpretation of the SMFS results.

Given that the soft long linkers used in SMFS experiments can drastically change the loading dynamics of the bond and influence the value of the rupture forces,[77] we are presently studying such effects theoretically, using both static and steered dynamical approaches. With such compliant linkers, it is also known that the recombination is facilitated. We have shown previously that the increase of force quickly after bond rupture when using long linkers does not preclude the recombination of bonds.[32, 33, 78] Computational studies of the linker role are clearly needed. They however remain challenging. This topic deserves a separate investigation that will be reported in a subsequent publication.

Acknowledgements

The research was funded by the Excellence of Science (EOS 40007519) program from the FWO and FRS-FNRS and the European Research Council (ERC Advanced Grant 101054338 to ASD). Computational resources have been provided by the Consortium des Equipements de Calcul Intensif (CECI), funded by the F.R.S.-FNRS under Grant # 2.5020. All the authors would like to thank Manuel Cardosa for useful discussions.

Supporting Information description: Additional details on the electronic structure, solvation models, thermochemistry, additional figures and tables for the geometries of other conformers, Molecular orbitals and mechanical response of the complexes.

TOC

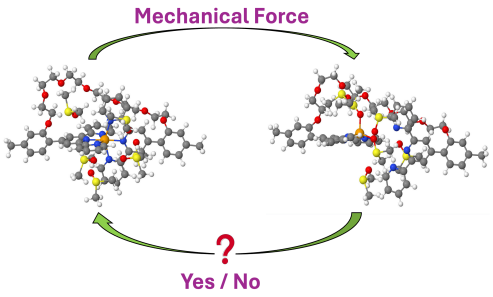

References

(1) De Bo, G. Polymer Mechanochemistry and the Emergence of the Mechanophore Concept. *Macromolecules* **2020**, *53* (18), 7615-7617. DOI: 10.1021/acs.macromol.0c01683.
(2) Chen, Y.; Mellot, G.; van Luijk, D.; Creton, C.; Sijbesma, R. P. Mechanochemical tools for polymer materials. *Chem. Soc. Rev.* **2021**, *50* (6), 4100-4140, 10.1039/D0CS00940G. DOI: 10.1039/D0CS00940G.
(3) Li, Y.; Zhu, C.; Dong, Y.; Liu, D. Supramolecular hydrogels: Mechanical strengthening with dynamics. *Polymer* **2020**, *210*, 122993. DOI: https://doi.org/10.1016/j.polymer.2020.122993.
(4) Qin, B.; Yin, Z.; Tang, X.; Zhang, S.; Wu, Y.; Xu, J.-F.; Zhang, X. Supramolecular polymer chemistry: From structural control to functional assembly. *Progress in Polymer Science* **2020**, *100*, 101167. DOI: https://doi.org/10.1016/j.progpolymsci.2019.101167.
(5) Voorhaar, L.; Hoogenboom, R. Supramolecular polymer networks: hydrogels and bulk materials. *Chem. Soc. Rev.* **2016**, *45* (14), 4013-4031, 10.1039/C6CS00130K. DOI: 10.1039/C6CS00130K.
(6) Chakma, P.; Konkolewicz, D. Dynamic Covalent Bonds in Polymeric Materials. *Angew. Chem. Int. Ed.* **2019**, *58* (29), 9682-9695, https://doi.org/10.1002/anie.201813525. DOI: https://doi.org/10.1002/anie.201813525 (acccessed 2021/02/07).

(7) Zhang, Z. P.; Rong, M. Z.; Zhang, M. Q. Polymer engineering based on reversible covalent chemistry: A promising innovative pathway towards new materials and new functionalities. *Progress in Polymer Science* **2018**, *80*, 39-93. DOI: https://doi.org/10.1016/j.progpolymsci.2018.03.002.
(8) Podgórski, M.; Fairbanks, B. D.; Kirkpatrick, B. E.; McBride, M.; Martinez, A.; Dobson, A.; Bongiardina, N. J.; Bowman, C. N. Toward Stimuli-Responsive Dynamic Thermosets through Continuous Development and Improvements in Covalent Adaptable Networks (CANs). *Adv. Mater.* **2020**, *32* (20), 1906876. DOI: https://doi.org/10.1002/adma.201906876 (acccessed 2024/09/28).
(9) Van Zee, N. J.; Nicolaÿ, R. Vitrimers: Permanently crosslinked polymers with dynamic network topology. *Progress in Polymer Science* **2020**, *104*, 101233. DOI: https://doi.org/10.1016/j.progpolymsci.2020.101233.
(10) O'Neill, R. T.; Boulatov, R. The many flavours of mechanochemistry and its plausible conceptual underpinnings. *Nat. Rev. Chem.* **2021**, *5* (3), 148-167. DOI: 10.1038/s41570-020-00249-y.
(11) Fantner, G. E.; Oroudjev, E.; Schitter, G.; Golde, L. S.; Thurner, P.; Finch, M. M.; Turner, P.; Gutsmann, T.; Morse, D. E.; Hansma, H.; et al. Sacrificial Bonds and Hidden Length: Unraveling Molecular Mesostructures in Tough Materials. *Biophys. J.* **2006**, *90* (4), 1411-1418. DOI: https://doi.org/10.1529/biophysj.105.069344.
(12) Barthelat, F.; Yin, Z.; Buehler, M. J. Structure and mechanics of interfaces in biological materials. *Nature Reviews Materials* **2016**, *1* (4), 16007. DOI: 10.1038/natrevmats.2016.7.
(13) Wegst, U. G. K.; Bai, H.; Saiz, E.; Tomsia, A. P.; Ritchie, R. O. Bioinspired structural materials. *Nat. Mater.* **2015**, *14* (1), 23-36. DOI: 10.1038/nmat4089.
(14) Zhou, X.; Guo, B.; Zhang, L.; Hu, G.-H. Progress in bio-inspired sacrificial bonds in artificial polymeric materials. *Chem. Soc. Rev.* **2017**, *46* (20), 6301-6329, 10.1039/C7CS00276A. DOI: 10.1039/C7CS00276A.
(15) Gu, Y.; Zhao, J.; Johnson, J. A. Polymer Networks: From Plastics and Gels to Porous Frameworks. *Angew. Chem. Int. Ed.* **2020**, *59* (13), 5022-5049. DOI: https://doi.org/10.1002/anie.201902900 (acccessed 2024/09/28).
(16) Li, J.; Nagamani, C.; Moore, J. S. Polymer Mechanochemistry: From Destructive to Productive. *Acc. Chem. Res.* **2015**, *48* (8), 2181-2190. DOI: 10.1021/acs.accounts.5b00184.
(17) Boulatov, R. Polymer Mechanochemistry. Springer: Cham, 2015.
(18) Mai, D. J.; Schroeder, C. M. 100th Anniversary of Macromolecular Science Viewpoint: Single-Molecule Studies of Synthetic Polymers. *ACS Macro Letters* **2020**, *9* (9), 1332-1341. DOI: 10.1021/acsmacrolett.0c00523.
(19) O'Neill, R. T.; Boulatov, R. Mechanochemical Approaches to Fundamental Studies in Soft-Matter Physics. *Angew. Chem. Int. Ed.* **2024**, *63* (19), e202402442. DOI: https://doi.org/10.1002/anie.202402442.
(20) Martínez-Tong, D. E.; Pomposo, J. A.; Verde-Sesto, E. Triggering Forces at the Nanoscale: Technologies for Single-Chain Mechanical Activation and Manipulation. *Macromol. Rapid Commun.* **2021**, *42* (1), 2000654. DOI: https://doi.org/10.1002/marc.202000654.
(21) Garcia-Manyes, S.; Beedle, A. E. M. Steering chemical reactions with force. *Nat. Rev. Chem.* **2017**, *1* (11), 0083. DOI: 10.1038/s41570-017-0083.

(22) Duwez, A.-S.; Cuenot, S.; Jérôme, C.; Gabriel, S.; Jérôme, R.; Rapino, S.; Zerbetto, F. Mechanochemistry: targeted delivery of single molecules. *Nat. Nanotechnol.* **2006**, *1* (2), 122-125. DOI: 10.1038/nnano.2006.92.
(23) Beyer, M. K.; Clausen-Schaumann, H. Mechanochemistry: The Mechanical Activation of Covalent Bonds. *Chem. Rev.* **2005**, *105* (8), 2921-2948. DOI: 10.1021/cr030697h.
(24) Kersey, F. R.; Yount, W. C.; Craig, S. L. Single-Molecule Force Spectroscopy of Bimolecular Reactions: System Homology in the Mechanical Activation of Ligand Substitution Reactions. *J. Am. Chem. Soc.* **2006**, *128* (12), 3886-3887. DOI: 10.1021/ja058516b.
(25) Hao, X.; Zhu, N.; Gschneidtner, T.; Jonsson, E. Ö.; Zhang, J.; Moth-Poulsen, K.; Wang, H.; Thygesen, K. S.; Jacobsen, K. W.; Ulstrup, J.; et al. Direct measurement and modulation of single-molecule coordinative bonding forces in a transition metal complex. *Nat. Commun* **2013**, *4* (1), 2121. DOI: 10.1038/ncomms3121.
(26) Kudera, M.; Eschbaumer, C.; Gaub, H. E.; Schubert, U. S. Analysis of Metallo-Supramolecular Systems Using Single-Molecule Force Spectroscopy. *Adv. Funct. Mater.* **2003**, *13* (8), 615-620. DOI: https://doi.org/10.1002/adfm.200304359.
(27) Wang, J.; Kouznetsova, T. B.; Niu, Z.; Ong, M. T.; Klukovich, H. M.; Rheingold, A. L.; Martinez, T. J.; Craig, S. L. Inducing and quantifying forbidden reactivity with single-molecule polymer mechanochemistry. *Nat. Chem* **2015**, *7* (4), 323-327. DOI: 10.1038/nchem.2185.
(28) Pill, M. F.; Holz, K.; Preußke, N.; Berger, F.; Clausen-Schaumann, H.; Lüning, U.; Beyer, M. K. Mechanochemical Cycloreversion of Cyclobutane Observed at the Single Molecule Level. *Chem. Euro. J.* **2016**, *22* (34), 12034-12039. DOI: 10.1002/chem.201600866.
(29) Li, H.; Walker, G. C. Twist and Shout: Single-Molecule Mechanochemistry. *ACS Nano* **2017**, *11* (1), 28-30. DOI: 10.1021/acsnano.6b08562.
(30) Calvaresi, M.; Duwez, A.-S.; Leigh, D. A.; Sluysmans, D.; Song, Y.; Zerbetto, F.; Zhang, L. Mechanical tightening of a synthetic molecular knot. *Chem* **2023**, *9* (1), 65-75. DOI: 10.1016/j.chempr.2022.12.014 (acccessed 2024/09/28).
(31) Van Quaethem, A.; Lussis, P.; Leigh, D. A.; Duwez, A.-S.; Fustin, C.-A. Probing the mobility of catenane rings in single molecules. *Chem. Sci.* **2014**, *5* (4), 1449-1452, 10.1039/C3SC53113A. DOI: 10.1039/C3SC53113A.
(32) Sluysmans, D.; Lussis, P.; Fustin, C.-A.; Bertocco, A.; Leigh, D. A.; Duwez, A.-S. Real-Time Fluctuations in Single-Molecule Rotaxane Experiments Reveal an Intermediate Weak Binding State during Shuttling. *J. Am. Chem. Soc.* **2021**, *143* (5), 2348-2352. DOI: 10.1021/jacs.0c12161.
(33) Sluysmans, D.; Hubert, S.; Bruns, C. J.; Zhu, Z.; Stoddart, J. F.; Duwez, A.-S. Synthetic oligorotaxanes exert high forces when folding under mechanical load. *Nat. Nanotechnol.* **2018**, *13* (3), 209-213. DOI: 10.1038/s41565-017-0033-7.
(34) Mughal, E. U.; Mirzaei, M.; Sadiq, A.; Fatima, S.; Naseem, A.; Naeem, N.; Fatima, N.; Kausar, S.; Altaf, A. A.; Zafar, M. N.; et al. Terpyridine-metal complexes: effects of different substituents on their physico-chemical properties and density functional theory studies. *R. Soc. Open Sci.* **2020**, *7* (11), 201208. DOI: 10.1098/rsos.201208 (acccessed 2024/09/28).

(35) Winter, A.; Newkome, G. R.; Schubert, U. S. Catalytic Applications of Terpyridines and their Transition Metal Complexes. *ChemCatChem* **2011**, *3* (9), 1384-1406. DOI: https://doi.org/10.1002/cctc.201100118 (acccessed 2024/09/28).
(36) Baranoff, E.; Collin, J.-P.; Flamigni, L.; Sauvage, J.-P. From ruthenium(ii) to iridium(iii): 15 years of triads based on bis-terpyridine complexes. *Chem. Soc. Rev.* **2004**, *33* (3), 147-155, 10.1039/B308983E. DOI: 10.1039/B308983E.
(37) Durot, S.; Reviriego, F.; Sauvage, J.-P. Copper-complexed catenanes and rotaxanes in motion: 15 years of molecular machines. *Dalton Trans.* **2010**, *39* (44), 10557-10570, 10.1039/C0DT00457J. DOI: 10.1039/C0DT00457J.
(38) Zhang, Q.; Tian, X.; Hu, Z.; Brommesson, C.; Wu, J.; Zhou, H.; Li, S.; Yang, J.; Sun, Z.; Tian, Y.; et al. A series of Zn(ii) terpyridine complexes with enhanced two-photon-excited fluorescence for in vitro and in vivo bioimaging. *J. Mater. Chem* **2015**, *3* (36), 7213-7221, 10.1039/C5TB01185J. DOI: 10.1039/C5TB01185J.
(39) Li, J.; Liu, R.; Jiang, J.; Liang, X.; Huang, L.; Huang, G.; Chen, H.; Pan, L.; Ma, Z. Zinc(II) Terpyridine Complexes: Substituent Effect on Photoluminescence, Antiproliferative Activity, and DNA Interaction. *Molecules* **2019**, *24* (24), 4519.
(40) Rossow, T.; Seiffert, S. Supramolecular polymer gels with potential model-network structure. *Polym. Chem.* **2014**, *5* (8), 3018-3029, 10.1039/C3PY01692G. DOI: 10.1039/C3PY01692G.
(41) Laquerbe, S.; Es Sayed, J.; Lorthioir, C.; Meyer, C.; Narita, T.; Ducouret, G.; Perrin, P.; Sanson, N. Supramolecular Crosslinked Hydrogels: Similarities and Differences with Chemically Crosslinked Hydrogels. *Macromolecules* **2023**, *56* (18), 7406-7418. DOI: 10.1021/acs.macromol.3c00769.
(42) Lewis, Reece W.; Malic, N.; Saito, K.; Evans, R. A.; Cameron, N. R. Ultra-high molecular weight linear coordination polymers with terpyridine ligands. *Chem. Sci.* **2019**, *10* (24), 6174-6183, 10.1039/C9SC01115C. DOI: 10.1039/C9SC01115C.
(43) Duan, H.-Y.; Wang, Y.-X.; Wang, L.-J.; Min, Y.-Q.; Zhang, X.-H.; Du, B.-Y. An Investigation of the Selective Chain Scission at Centered Diels–Alder Mechanophore under Ultrasonication. *Macromolecules* **2017**, *50* (4), 1353-1361. DOI: 10.1021/acs.macromol.6b02370.
(44) Yang, H.; Ghiassinejad, S.; van Ruymbeke, E.; Fustin, C.-A. Tunable Interpenetrating Polymer Network Hydrogels Based on Dynamic Covalent Bonds and Metal–Ligand Bonds. *Macromolecules* **2020**, *53* (16), 6956-6967. DOI: 10.1021/acs.macromol.0c00494.
(45) Jakobs, R. T. M.; Sijbesma, R. P. Mechanical Activation of a Latent Olefin Metathesis Catalyst and Persistence of its Active Species in ROMP. *Organometallics* **2012**, *31* (6), 2476-2481. DOI: 10.1021/om300161z.
(46) Sammon, M. S.; Biewend, M.; Michael, P.; Schirra, S.; Ončák, M.; Binder, W. H.; Beyer, M. K. Activation of a Copper Biscarbene Mechano-Catalyst Using Single-Molecule Force Spectroscopy Supported by Quantum Chemical Calculations. *Chemistry – A European Journal* **2021**, *27* (34), 8723-8729. DOI: https://doi.org/10.1002/chem.202100555.
(47) Beyer, M. K. The mechanical strength of a covalent bond calculated by density functional theory. *J. Chem. Phys.* **2000**, *112*, 7307-7312. DOI: 10.1063/1.481330.
(48) Chung, L. W.; Sameera, W. M. C.; Ramozzi, R.; Page, A. J.; Hatanaka, M.; Petrova, G. P.; Harris, T. V.; Li, X.; Ke, Z.; Liu, F.; et al. The ONIOM Method and Its Applications. *Chem. Rev.* **2015**, *115* (12), 5678-5796. DOI: 10.1021/cr5004419.

(49) Mennucci, B. Polarizable continuum model. *WIREs Computational Molecular Science* **2012**, *2* (3), 386-404. DOI: https://doi.org/10.1002/wcms.1086 (acccessed 2024/09/28).
(50) Frisch, M. J.; Trucks, G. W.; Schlegel, H. B.; Scuseria, G. E.; Robb, M. A.; Cheeseman, J. R.; Scalmani, G.; Barone, V.; Petersson, G. A.; Nakatsuji, H.; et al. *Gaussian 16 Rev. C.01*; Wallingford, CT; Gaussian Inc., 2016.
(51) Perdew, J. P.; Burke, K.; Ernzerhof, M. Generalized Gradient Approximation Made Simple. *Phys. Rev. Lett.* **1996**, *77* (18), 3865-3868. DOI: 10.1103/PhysRevLett.77.3865.
(52) Zhao, Y.; Truhlar, D. G. The M06 suite of density functionals for main group thermochemistry, thermochemical kinetics, noncovalent interactions, excited states, and transition elements: two new functionals and systematic testing of four M06-class functionals and 12 other functionals. *Theor. Chem. Acc.* **2008**, *120* (1), 215-241. DOI: 10.1007/s00214-007-0310-x.
(53) Grimme, S. Semiempirical GGA-type density functional constructed with a long-range dispersion correction. *Journal of Computational Chemistry* **2006**, *27* (15), 1787-1799. DOI: https://doi.org/10.1002/jcc.20495.
(54) Chai, J.-D.; Head-Gordon, M. Long-range corrected hybrid density functionals with damped atom–atom dispersion corrections. *Phys. Chem. Chem. Phys.* **2008**, *10* (44), 6615-6620, 10.1039/B810189B. DOI: 10.1039/B810189B.
(55) Hsu, T.-W.; Hsu, H.-C.; Chan, H.-Y.; Fang, J.-M. A Terpyridine Zinc Complex for Selective Detection of Lipid Pyrophosphates: A Model System for Monitoring Bacterial O- and N-Transglycosylations. *J. Org. Chem.* **2020**, *85* (19), 12747-12753. DOI: 10.1021/acs.joc.0c01252.
(56) Svensson, M.; Humbel, S.; Froese, R. D. J.; Matsubara, T.; Sieber, S.; Morokuma, K. ONIOM: A Multilayered Integrated MO + MM Method for Geometry Optimizations and Single Point Energy Predictions. A Test for Diels−Alder Reactions and Pt(P(t-Bu)3)2 + H2 Oxidative Addition. *J. Phys. Chem.* **1996**, *100* (50), 19357-19363. DOI: 10.1021/jp962071j.
(57) Vreven, T.; Byun, K. S.; Komáromi, I.; Dapprich, S.; Montgomery, J. A., Jr.; Morokuma, K.; Frisch, M. J. Combining Quantum Mechanics Methods with Molecular Mechanics Methods in ONIOM. *J. Chem. Theor. Comp.* **2006**, *2* (3), 815-826. DOI: 10.1021/ct050289g.
(58) Tomasi, J.; Mennucci, B.; Cammi, R. Quantum Mechanical Continuum Solvation Models. *Chem. Rev.* **2005**, *105* (8), 2999-3094. DOI: 10.1021/cr9904009.
(59) Cancès, E.; Mennucci, B.; Tomasi, J. A new integral equation formalism for the polarizable continuum model: Theoretical background and applications to isotropic and anisotropic dielectrics. *J. Chem. Phys.* **1997**, *107* (8), 3032-3041. DOI: 10.1063/1.474659 (acccessed 9/2/2024).
(60) Stauch, T.; Dreuw, A. Advances in Quantum Mechanochemistry: Electronic Structure Methods and Force Analysis. *Chem. Rev.* **2016**, *116* (22), 14137-14180. DOI: 10.1021/acs.chemrev.6b00458.
(61) Ong, M. T.; Leiding, J.; Tao, H.; Virshup, A. M.; Martínez, T. J. First Principles Dynamics and Minimum Energy Pathways for Mechanochemical Ring Opening of Cyclobutene. *J. Am. Chem. Soc.* **2009**, *131* (18), 6377-6379. DOI: 10.1021/ja8095834.
(62) Ribas-Arino, J.; Shiga, M.; Marx, D. Understanding Covalent Mechanochemistry. *Angew. Chem. Int. Ed.* **2009**, *48* (23), 4190-4193. DOI: https://doi.org/10.1002/anie.200900673.

(63) Wolinski, K.; Baker, J. Theoretical predictions of enforced structural changes in molecules. *Molecular Physics* **2009**, *107* (22), 2403-2417. DOI: 10.1080/00268970903321348.
(64) Presselt, M.; Dietzek, B.; Schmitt, M.; Popp, J.; Winter, A.; Chiper, M.; Friebe, C.; Schubert, U. S. Zinc(II) Bisterpyridine Complexes: The Influence of the Cation on the π-Conjugation between Terpyridine and the Lateral Phenyl Substituent. *J. Phys. Chem. C* **2008**, *112* (47), 18651-18660. DOI: 10.1021/jp807461j.
(65) Chen, X.; Zhou, Q.; Cheng, Y.; Geng, Y.; Ma, D.; Xie, Z.; Wang, L. Synthesis, structure and luminescence properties of zinc (II) complexes with terpyridine derivatives as ligands. *Journal of Luminescence* **2007**, *126* (1), 81-90. DOI: https://doi.org/10.1016/j.jlumin.2006.05.008.
(66) Tang, L.; Yang, X.-G.; Li, D.-S.; Wang, J.-J.; Gao, X.-M.; Wang, J.-W. Crystal structure of bis(2,2':6',2'-terpyridine)zinc(II) dinitrate dihydrate, [Zn(C15H11N3)2][NO3]2 · 2H2O. *Zeitschrift für Kristallographie - New Crystal Structures* **2007**, *222* (1), 59-60. DOI: doi:10.1524/ncrs.2007.0022 (acccessed 2025-02-26).
(67) Pracht, P.; Bohle, F.; Grimme, S. Automated exploration of the low-energy chemical space with fast quantum chemical methods. *Phys. Chem. Chem. Phys.* **2020**, *22* (14), 7169-7192, 10.1039/C9CP06869D. DOI: 10.1039/C9CP06869D.
(68) Pracht, P.; Grimme, S.; Bannwarth, C.; Bohle, F.; Ehlert, S.; Feldmann, G.; Gorges, J.; Müller, M.; Neudecker, T.; Plett, C.; et al. CREST—A program for the exploration of low-energy molecular chemical space. *J. Chem. Phys.* **2024**, *160* (11), 114110. DOI: 10.1063/5.0197592 (acccessed 3/7/2025).
(69) Bannwarth, C.; Ehlert, S.; Grimme, S. GFN2-xTB—An Accurate and Broadly Parametrized Self-Consistent Tight-Binding Quantum Chemical Method with Multipole Electrostatics and Density-Dependent Dispersion Contributions. *J. Chem. Theor. Comp.* **2019**, *15* (3), 1652-1671. DOI: 10.1021/acs.jctc.8b01176.
(70) Grimme, S. Exploration of Chemical Compound, Conformer, and Reaction Space with Meta-Dynamics Simulations Based on Tight-Binding Quantum Chemical Calculations. *J. Chem. Theor. Comp.* **2019**, *15* (5), 2847-2862. DOI: 10.1021/acs.jctc.9b00143.
(71) Zhang, H.; Li, X.; Lin, Y.; Gao, F.; Tang, Z.; Su, P.; Zhang, W.; Xu, Y.; Weng, W.; Boulatov, R. Multi-modal mechanophores based on cinnamate dimers. *Nat. Commun* **2017**, *8* (1), 1147. DOI: 10.1038/s41467-017-01412-8.
(72) Brown, C. L.; Bowser, B. H.; Meisner, J.; Kouznetsova, T. B.; Seritan, S.; Martinez, T. J.; Craig, S. L. Substituent Effects in Mechanochemical Allowed and Forbidden Cyclobutene Ring-Opening Reactions. *J. Am. Chem. Soc.* **2021**, *143* (10), 3846-3855. DOI: 10.1021/jacs.0c12088.
(73) Zhang, Y.; Wang, Z.; Kouznetsova, T. B.; Sha, Y.; Xu, E.; Shannahan, L.; Fermen-Coker, M.; Lin, Y.; Tang, C.; Craig, S. L. Distal conformational locks on ferrocene mechanophores guide reaction pathways for increased mechanochemical reactivity. *Nat. Chem* **2021**, *13* (1), 56-62. DOI: 10.1038/s41557-020-00600-2.
(74) Qian, H.; Purwanto, N. S.; Ivanoff, D. G.; Halmes, A. J.; Sottos, N. R.; Moore, J. S. Fast, reversible mechanochromism of regioisomeric oxazine mechanophores: Developing in situ responsive force probes for polymeric materials. *Chem* **2021**, *7* (4), 1080-1091. DOI: https://doi.org/10.1016/j.chempr.2021.02.014.
(75) Cardosa-Gutierrez, M.; De Bo, G.; Duwez, A.-S.; Remacle, F. Bond breaking of furan–maleimide adducts via a diradical sequential mechanism under an external mechanical

force. *Chem. Sci.* **2023**, *14* (5), 1263-1271, 10.1039/D2SC05051J. DOI: 10.1039/D2SC05051J.
(76) Chu, T.; Belding, L.; Poddutoori, P. K.; van der Est, A.; Dudding, T.; Korobkov, I.; Nikonov, G. I. Unique molecular geometries of reduced 4- and 5-coordinate zinc complexes stabilised by diiminopyridine ligand. *Dalton Trans.* **2016**, *45* (34), 13440-13448, 10.1039/C6DT02001A. DOI: 10.1039/C6DT02001A.
(77) Evans, E.; Ritchie, K. Strength of a Weak Bond Connecting Flexible Polymer Chains. *Biophys. J.* **1999**, *76* (5), 2439-2447. DOI: https://doi.org/10.1016/S0006-3495(99)77399-6.
(78) Sluysmans, D.; Devaux, F.; Bruns, C. J.; Stoddart, J. F.; Duwez, A.-S. Dynamic force spectroscopy of synthetic oligorotaxane foldamers. *Proceedings of the National Academy of Sciences* **2018**, *115* (38), 9362-9366. DOI: 10.1073/pnas.1712790115 (acccessed 2025/03/09).